ELSEVIER

Physica E 6 (2000) 821–827

PHYSICA E

www.elsevier.nl/locate/physe

Charge detection with nanomechanical resonators

R.H. Blick*, A. Erbe, H. Krömmer, A. Kraus, J.P. Kotthaus

Center for Nanoscience and Sektion Physik, Ludwig-Maximilians-Universität, Geschwister-Scholl-Platz 1, 80539 München, Germany

Abstract

We report on our recent work on nanomachined electromechanical resonators applied as mechanically flexible beams and tunneling contacts operating in the radio frequency regime. We discuss as to how to build Au/Si beams of length varying from 1 to 4 μm and width down to only 80 nm. We show how to apply them as charge detectors and how to drive the freely suspended beams into nonlinear response. This not only enables extremely sensitive charge detection, but also allows investigations of nonlinear dynamics in mechanical systems close to the quantum limit. Furthermore, we demonstrate how these nanometer devices can be used to mechanically transfer only a few electrons in each cycle of operation.

PACS: 07.10.Cm; 77.65.Fs; 73.40.Gk

Keywords: Charge detection; Nanomechanical resonators

Measuring charge nowadays is commonly performed with electronic solid-state devices, like field-effect transistors. However, the classical approach developed by Coulomb in the 18th century [1] is based on a mechanical electrometer. In the present work we want to demonstrate how nanomechanical devices can be applied for charge detection. The advantages of these systems are clearly given by their speed of operation in the radio frequency (RF) range and, as will be discussed, their sensitivity.

As everyone knows, the audible sounds of a guitar are generated by the clamped strings. By halving such a string, the eigenfrequencies are increased by an octave. Scaling down the string to only some 100 nm yields frequencies in the RF range. Recent work on such nanomechanical resonators [2–4] demonstrated their versatility, although not for musicians, but for applications in metrology. Integrating mechanically flexible structures with single-electron devices or two-dimensional electron gases [5] on the nanometer scale offers not only high speed of operation but also broad tunability of the tunneling contacts. This is of great interest regarding electrometry with single-electron devices, which are currently limited to operating frequencies of 10 MHz and extremely low temperatures (<10 mK). Applications of mechanical resonators in nonlinear oscillators [6] or parametric amplifiers [7] are of great importance for scanning probe measurements and accurate frequency counters or clocks in general.

In this first part, we demonstrate as to how to observe the nonlinear response of such nanomechanical resonators and how to apply these devices for

* Corresponding author. Tel.: +49-89-2180-3733; fax: +49-89-2180-3182.

E-mail address: robert.blick@physik.uni-muenchen.de (R.H. Blick)

1386-9477/00/$ - see front matter
PII: S1386-9477(99)00250-7

charge detection. The resonators are operated in the RF regime with typical dimensions of only a few 100 nm in width and height. On applying a sufficiently large excitation amplitude the suspended beam shows a highly nonlinear response, which in turn allows extremely sensitive charge detection. Moreover, the device represents a model to study phenomena such as stochastic resonance and deterministic chaos in a mechanical system on the nanometer scale.

The samples were machined out of single-crystal silicon-on-insulator (SOI) substrates by a combined dry- and wet-etch process. The SOI substrate consists of a 190 nm thick silicon layer, a 390 nm SiO_2 sacrificial layer and a semi-insulating Si wafer material. In a first step optical lithography was performed defining metallic gates and pads capable of supporting radio and microwave frequencies. In a second step we used electron-beam lithography to define the metallic nanostructure. The metal layers deposited on Si during lithography are a thin adhesion layer of Ni/Cr (1.5 nm), a covering Au layer (~ 50 nm), and an Al etch mask (30 nm). A reactive-ion etch was then applied to mill down the silicon by 600 nm not covered with metal. Finally, the sample was etched in diluted HF, defining the suspended silicon layer with a thickness of 190 nm. One of the suspended resonators is shown in Fig. 1: The beam has a length of almost 3 μm, a width of $w = 200$ nm and a height of $h = 250$ nm and is clamped on both sides. The gate contact couples capacitively to the resonator.

All measurements shown in this case were conducted at 4.2 K in a sample holder with a residual ^{4}He gas pressure of about 10^{-2} mbar. The sample was mounted between interconnecting microstrip lines, designed to feed the circuit with frequencies up to 10 GHz, and then aligned in parallel with the externally applied magnetic field. The absolute resistance of the metal wire on top of the resonator was found to be 30 Ω, which results in a fairly well-defined impedance matching of the whole circuit. In contrast to the electrostatic excitation of motion in case of the quantum bell discussed later on, the beam is now set into

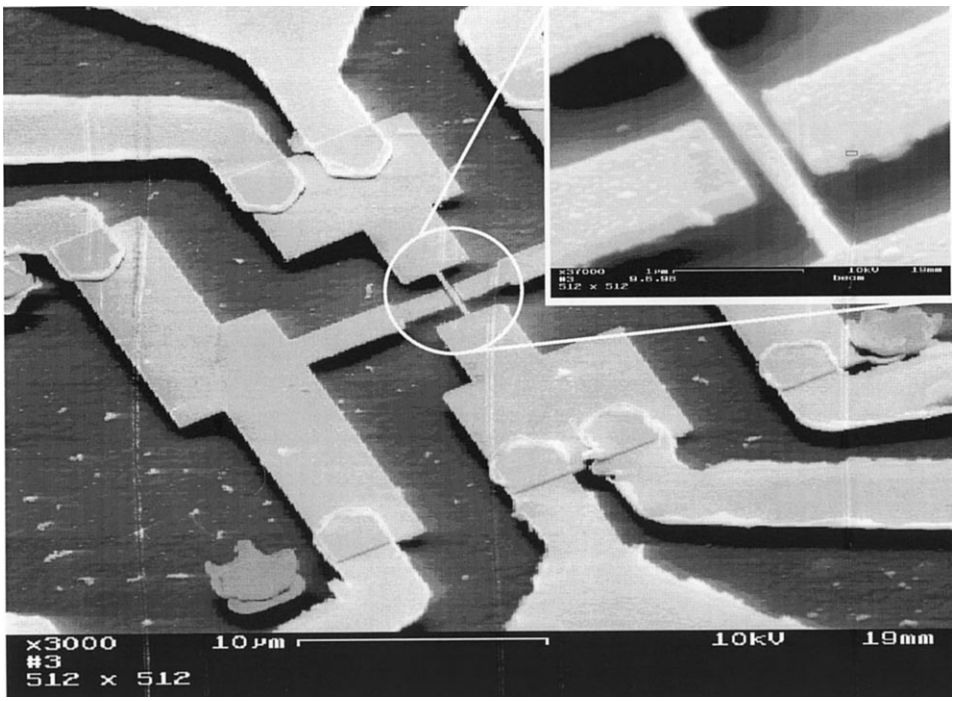

Fig. 1. Micrograph of a nanomechanical resonator, machined out of Si with a 100 nm evaporated Au layer. The center gates couple capacitively to the resonator. The inset shows a close-up of the suspended beam.

motion by applying a high-frequency electromagnetic excitation and ramping the magnetic field in plane. This results in an effective Lorentz force generated perpendicular to the sample surface. The response of the beam is finally probed with a spectrum analyzer, measuring directly the electromagnetic power absorbed by the motion of the beam. The preamplifier employed is a low-noise broad-band (UHF- to L-band) JS amplifier with a specified noise figure of NF = 0.6 dB and a gain of $G = 30$ dB.

The onset of the resonance dependent on the magnetic field is depicted in Fig. 2(a): With increasing magnetic field the peak is more pronounced; it varies as B^2. The driving amplitude in this case is -66 dB m – the quality factor obtained is $Q = f/\delta f = 2.3 \times 10^3$. In order to estimate effective attenuation by the ^{4}He coupling gas, we varied the residual pressure. We found that the maximum resonance amplitude is already sensitively reduced by small amounts of gas. Liquid ^{4}He can damp out the mechanical motion completely [8].

The capacitive coupling between beam and gate is determined by numerical evaluation, as noted before. From these calculations we obtain a capacitive coupling between gate and beam in the linear regime of $C_{gb} \cong 220$ aF. The frequency shift δf of the mechanical resonance is found to be

$$\delta f = \sqrt{f^2 - \frac{C''(0)}{2m_{\text{eff}}}V^2} - f \cong \frac{C''(0)}{4m_{\text{eff}}f^2}V^2, \qquad (1)$$

where m_{eff} is the beam's effective mass (in our case $\sim 4.3 \times 10^{-16}$ kg), V the applied gate voltage, and C'' represents the second derivative of the capacitance with respect to the spatial coordinate. It has to be noted that for an absolute charge measurement the necessary charging of all the metallic contacts, e.g. bond pads and leads have to be taken into account. For one of the bond pads, for example, we estimate a capacitance of $C_{bp} = \varepsilon A/d \cong 2.11$ fF. However, it is still possible to determine the relative charge δ_q on the closely connected gate with a high accuracy [9,10].

The nonlinearity found in the beam response (see Fig. 2(b)) is caused by the variation of the restoring force at the clamping points [3] and can be modelled by adding a cubic term in the equation of motion of the beam [6]. On comparing the model derived by Greywall and Yurke [11] with our data we find excellent agreement. In a more detailed study of the nonlinear properties we found that it can even be used for the generation of 'mechanical' harmonics [12].

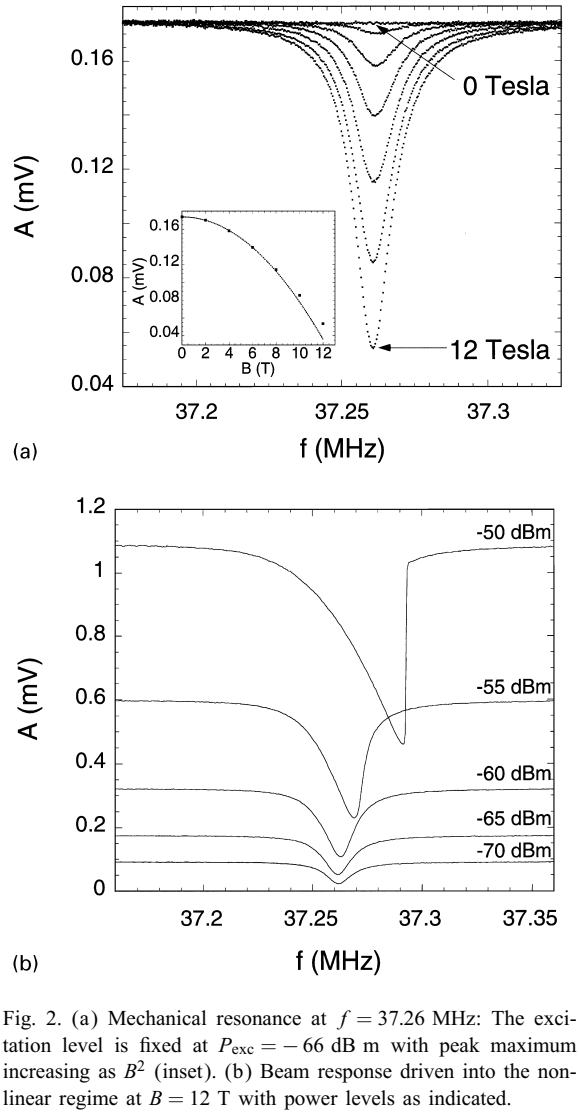

Fig. 2. (a) Mechanical resonance at $f = 37.26$ MHz: The excitation level is fixed at $P_{\text{exc}} = -66$ dB m with peak maximum increasing as B^2 (inset). (b) Beam response driven into the nonlinear regime at $B = 12$ T with power levels as indicated.

The best operating condition for electrometry are obtained by adjusting the amplitude at the critical point. The critical point for the traces shown in Fig. 3 is in the region of maximum slope. The excitation power is levelled at -52.8 dB m and the magnetic field at 12 T. As seen in the inset the peak position varies as the square of the gate voltage applied. We achieve a sensitivity of $\Delta V/\sqrt{\Delta f} \cong 4.1 \times 10^{-2}$ V/$\sqrt{\text{Hz}}$. The slope at the critical point $\mathrm{d}A/\mathrm{d}f|_{f=f_c} \to \infty$

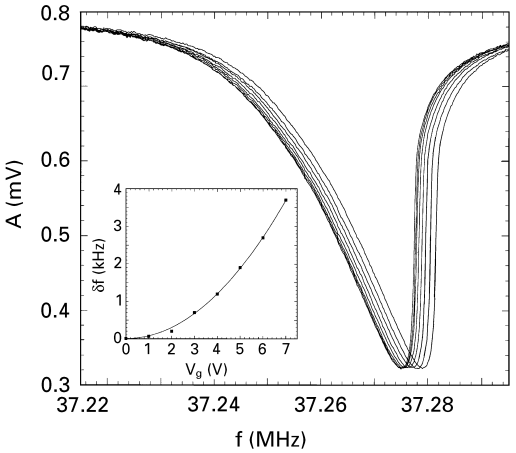

Fig. 3. Operating the resonator in the transition region at $P_{exc} = -52.8$ dB m with maximum signal sensitivity. Resonance traces are shifted by an applied gate voltage. The inset shows the frequency shift of the resonance with varying gate voltage.

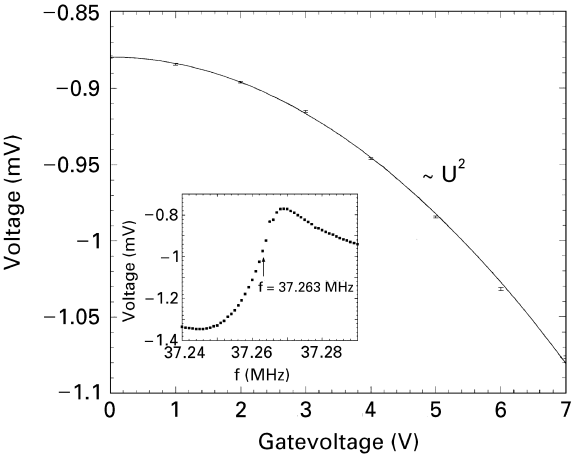

Fig. 4. Measured variation of the phase shift ($V \propto \delta\phi$) of the nanomechanical resonator in the transition region at $f = 37.263$ MHz. Inset: Measured phase shift when resonance is passed.

diverges resulting in extremely sensitive amplification. In the measurements presented we obtain a charge resolution at a finite bias on the gate ($V = \pm 4$ V) of $\sim 0.7 \times 10^2$ e/$\sqrt{\text{Hz}}$ limited by electronic noise. It is important to note the enhancement of sensitivity with increasing gate voltage (see the inset of Fig. 3).

The accuracy of the measurement can even be enhanced by determining the phase shift the mechanical resonance causes within the whole electrical circuit. For this measurement we modified our setup according to Ref. [2], i.e., including a mixer and a phase shifter. With this setup it was possible to obtain a sensitivity of $\sim 1.0 \times 10^{-1}$ e/$\sqrt{\text{Hz}}$. As before the operating point is adjusted in the transition region at the critical point, as seen in Fig. 4. The phase shift itself is proportional to $V \propto \delta\phi$, where V denotes the voltage applied on the gate contact.

As a second approach towards building electromechanical devices on the nanometer scale, we started off with a sample similar to the one shown in Fig. 1, but disconnected one of the clamping points. Hence, we ended up with a structure similar to a clapper in between two electrodes. At a certain voltage the mechanical clapper is pulled towards one of the electrodes and charge can flow onto the metallic link. The clapper itself is then pulled back by the mechanical restoring force and delivers the acquired charge to the grounded electrode. This process is periodically repeated and the clapper resonates or 'rings' much like a classical bell. Since the electrons's charge is quantized the configuration shown can in principle be used to count single electrons, much in the same way as in Millikan's famous experiment with oil drops [13] or by using single-electron transistors [14–18].

Here, we demonstrate a new technique for counting electrons with a mechanical resonator, which is based on a mechanically flexible tunneling contact. In the case of macroscopic bells the granularity of the charge carriers is not observed, due to the large currents applied. In the present case the underlying idea is to scale down a classical bell in order to build a 'quantum bell' with which single electrons can be transferred. Naturally, there are some differences between a classical bell and our resonator: We rely on radio frequency electrostatic excitation of the clapper and not on a small magnet. Moreover, the clapper shown in the scanning electron microscope (SEM) micrograph of Fig. 5 has a size of only 1000 nm × 150 nm × 190 nm (length × width × thickness), leading to eigenfrequencies up to 400 MHz. However, regarding the fundamental similarities we find that electrons are transferred by a mechanically flexible contact. Besides reducing the size of the resonator, a quantum bell requires tunneling contacts in order to achieve

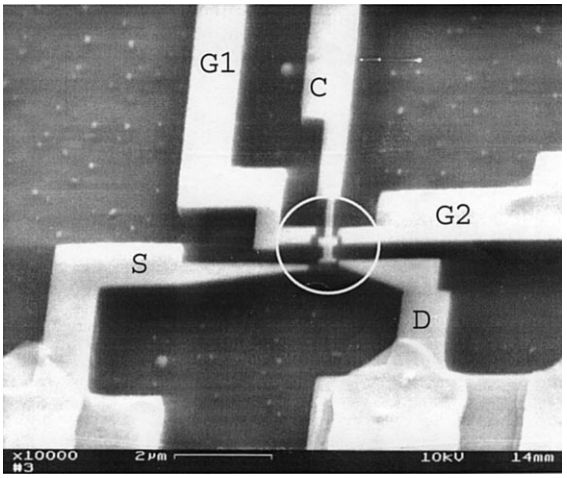

Fig. 5. A scanning electron beam micrograph of the suspended silicon structure covered by an evaporated metallic layer. The clapper in the center is undercut up to the second joint. The inset shows an electrical circuit diagram of the bell with drain (D), source (S), clapper (C) and gate contacts (#1 and #2). The clapper is biased and current flows through the drain contact. Radio frequencies are applied at gate contacts #1 and #2, while the source contact is grounded. The RF signal on gate #1 is phase shifted by $\phi = \pi$ to gate #2.

tunneling of only a few electrons in each cycle of motion onto and off the clapper. In Fig. 5 the contacts are marked as follows: drain (D) and source (S) tips function as tunneling contacts for the metallized Si clapper (C) in the center. The clapper can be adjusted by DC biasing the additional gate contacts #1 (G1) or #2 (G2). These two gate contacts (#1 and #2) allow effective capacitive radio frequency (RF) coupling, leading to an in-plane motion of the clapper between drain and source.

In the present measurements the RF modulation is applied to gates #1 and #2, while the source contact is grounded – the signal on gate #1 is phase shifted by $\phi = \pi$. We operate at frequencies up to some 100 MHz across the clapper electrode. Current then flows from the clapper to the drain contact and the DC current is finally amplified. The sample is mounted in a standard sample holder allowing measurements in vacuum and at low temperatures. The obtained DC I–V characteristic is shown in Fig. 6: At 300 K we find an exponential increase of the current with $V_{\text{clapper/drain}}$ when the clapper is pulled towards the drain contact around $V_{\text{clapper/drain}} \cong -1$ V. Electrons then tunnel across the

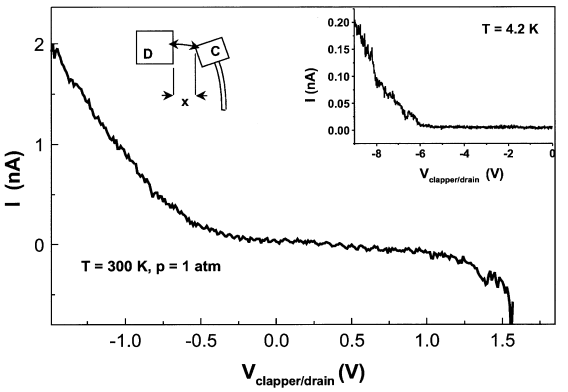

Fig. 6. Static I–V characteristic of the mechanical clapper without applying radio frequency. The DC current as a function of bias voltage across the clapper/drain contact at $T = 300$ K is plotted. The inset shows the I–V characteristic at 4.2 K.

gap. Further biasing of the clapper finally leads to a metallic contact. The upper right inset shows the same characteristic measured at 4.2 K: Clearly the onset of the tunneling current occurs at a larger bias voltage. The temperature dependence of the I–V characteristics can be explained by the enhanced Brownian motion and the reduced stiffness of the clapper at room temperature (no hysteresis is observed at 300 K).

At low temperatures we find a hysteresis from which we estimate the contact force to be of the order of ~330 nN (here we calibrated the displacement of the clapper with respect to drain voltage applied and used the spring constant for Si). The DC I–V response is not symmetrical when the current preamplifier is connected to the source contact. The measurements at low temperatures were performed after the sample holder was evacuated and a small amount of ^{4}He gas was introduced in order to enhance cooling. The pressure in the sample holder was thus around some 10 mbar. Interestingly this results in an increased noise presumeably caused by ionization of the gas in between the clapper and drain contact tips where the electric field gradient is maximum ($E_{\text{tip}} \sim 10^7$–10^8 V/m). Under ambient gas pressure this discharging at the contact tip is strongly reduced.

We have seen that the resistance of the contact (clapper/drain) depends exponentially on the tip displacement and hence on the distance to drain/source by $R(x(t)) = R_0 \exp(x(t)/\lambda)$. This can be adjusted by electrostatic tuning: λ is the material constant of the

metallic electrodes defined by $\lambda^{-1} = \sqrt{(2m_e\Phi)}/\hbar$, with Φ being the work function and m_e the electron mass. This allows a mechanical variation of the RC constant and hence the tunneling characteristics of the junction, which is not possible for common single-electron transistor (SET) devices. By applying radio frequencies up to 100 MHz across gate #1 and the source contact, we finally realize the nonomechanical resonator. We estimate the capacitance of the clapper tip to drain contact to be of the order of $C \approx 25$ aF. This estimation is based on calculations with electromagnetic problem solvers (MAFIA,ver.3.20, 1993). Combining the capacitance and the tunneling resistance found in DC measurements, we obtain an RC constant of $\tau \sim 25$ aF $\times$ 1 GΩ = 25 ns. Hence, the electrons are transferred one by one with a rate which can be approximated by the RC constant. The value of 25 ns corresponds to 40 MHz, which is the range of operation of our mechanical resonator. Therefore, the mechanical motion leads to a modulation or 'chopping' of the electron tunneling rate. Electron tunneling is a discrete process, as exemplified by shot noise [19]. Since we are able to modulate the resonator at this rate, we transfer only a small discrete number of electrons in each cycle of operation. In other words, the average current is given by $\langle I\rangle = \langle q\rangle f = \langle n\rangle ef$, where $\langle n\rangle$ is the average number of electrons being transferred at frequency f in each cycle.

A certain drawback of this mechanical resonator is the discrete set of eigenfrequencies. Accordingly, only a limited number of frequencies are available for electron transfer. On the other hand, this gives the flexibility to design a resonator with a specific mode spectrum in the radio frequency range only, which in turn minimizes 'leakage' currents in the low-frequency regime and the influence of $1/f$ noise. A simulation of the mechanical properties of our resonator is performed with a software package (MCS PATRAN, ver. 6.2), allowing us to test the influence of shape and clamping points on the eigenmodes of the device. Since the Au layer has almost the same thickness as the silicon supporting structure it is necessary to model a hybrid Au/Si system. This is done by simply assuming two rigidly coupled bars with different spring constant ($\kappa_{Au} = 0.38$ N/m, $\kappa_{Si} = 46$ N/m – these values include geometrical factors). The resulting eigenfrequency spectrum shows a strong resonant response

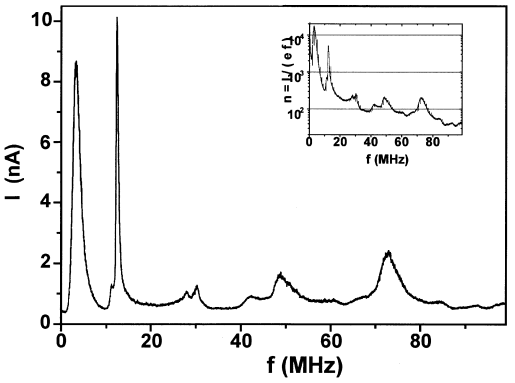

Fig. 7. Tunneling current through the clapper/drain contact plotted versus applied frequency (applied at gate contact #1 and #2). Several mechanical resonances up to 73 MHz with a quality factor of $Q \sim 100, 30$, and 15 are found (from left to right). Inset: Log plot of electron number versus frequency (for details see text). In the high-frequency peaks about 130 electrons are transferred in each cycle, which can be easily reduced to only 5 electrons/cycle at a reasonable signal/noise ratio.

between $f = 10$ and 100 MHz. It is obvious that the mass of the metallic layer on top reduces the attainable maximum frequency and the quality factor Q of our resonator ($Q = f/\delta f$). As expected, maximum strain is found at the clamping points, which further limits the performance (data not shown)

The RF response of the resonator is presented in Figs. 7 and 8 – it is obtained at 300 K under He^4 gas pressure of 1 bar and an excitation amplitude of $V_{RF}^{pp} = \pm 5$ V: The different traces in Fig. 8 correspond to various DC bias voltages on the clapper. As seen, we find a number of mechanical resonances with small quality factor Q of 100, 30, and 15 where the complex resonance structure is a result of the geometry of the clapper. Applying the relation for the average DC current $\langle I\rangle = \langle n\rangle ef$ (see the inset in Fig. 7). In the low-frequency resonances up to 10^4 electrons are transferred in each cycle, while at 73 MHz we find a transfer rate of $\sim$130 electrons at this amplitude of the driving voltage. The peak currents and the noise increase at larger bias voltages (0.1–0.5 V). It can also be seen that the background conductance increases. The peak values themselves show an exponential increase of the current with $V_{clapper/drain}$, which is shown in detail in the inset for the peak at $f = 73$ MHz. Here the solid line is an exponential fit to the data points.

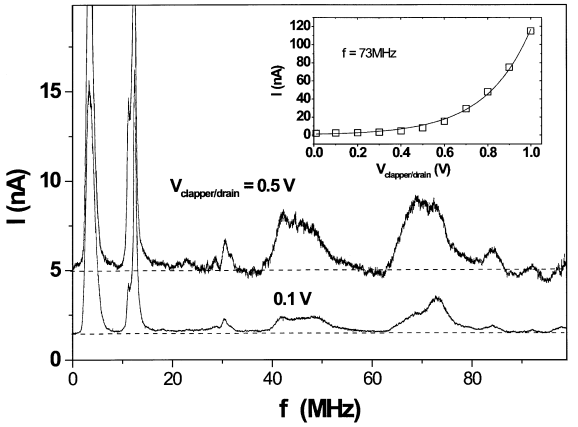

Fig. 8. Resonance curves at different values of the DC voltage bias across clapper/drain contact. The variation of the voltage bias results in an exponential increase of peak and background current. Inset: exponential increase of peak current at 73 MHz – the solid line is an exponential fit to the data points (open boxes).

From this exponential behavior of the peak current at 73 MHz shown in the inset of Fig. 8, we can estimate x, which gives a value for the distance between the clapper and drain contacts at the maximum applied DC voltage – we obtain $x_{max} \approx 5$ nm.

In conclusion, we demonstrated the operation of a variety of nanomechanical resonators. Our main focus is on the accurate detection of single-electron charges with the help of these mechanical devices. The main features are the high speed of operation and the increased sensitivity, due to the operation in the nonlinear regime. Furthermore, by scaling down a classical bell in size we have shown that a quantum bell can be built which rings in the ultrasonic frequency range. The essential requirement is a nanometer scale clapper resonating at radio frequencies and the ability to tune the RC constant of the tunneling contact. So far, we have obtained an accuracy of about ± 2 electrons, which can be transferred in a single revolution of the clapper. In the newly developed setup of the experiment we included a metallic island on the tip of the clapper, forming a metallic SET, in order to realize an electron shuttle mechanism, as proposed by Gorelik et al. [20]. A detailed theoretical description of this approach is already given by Weiss and Zwerger [21], indicating that such a mechanical single-electron shuttle should operate up to temperatures of 1 K. The Coulomb repulsion in this case functions as an additional energy barrier for electrons to tunnel onto the island.

Acknowledgements

We like to thank Ch. Weiss, W. Zwerger, and U. Sivan for valuable discussions. This work was funded in part by the Bundesministerium für Bildung, Wissenschaft, Forschung and Technologie (BMBF) and the Deutsche Forschungsgemeinschaft (DFG). The SOI wafers used to machine the quantum bell were donated by Siemens Corp., Germany.

References

[1] C.A. Coulomb, Memoires de I'Academie Royale des Sciences, 229, Academie royale des sciences, Paris (1784).
[2] A.N. Cleland, M.L. Roukes, Nature 392 (1998) 160.
[3] A.N. Cleland, M.L. Roukes, Appl. Phys. Lett. 69 (1996) 2653.
[4] A. Erbe, R.H. Blick, A. Tilke, A. Kriele, J.P. Kotthaus, Appl. Phys. Lett. 73 (1998) 3751.
[5] R.H. Blick, M.L. Roukes, W. Wegscheider, M. Bichler, Physica A 784 (1998) 249–251.
[6] D.S. Greywall, B. Yurke, P.A. Busch, A.N. Pargellis, R.L. Willett, Phys. Rev. Lett. 72 (1994) 2992.
[7] D. Rugar, P. Grütter, Phys. Rev. Lett. 67 (1991) 699.
[8] A. Kraus, A. Erbe, R.H. Blick, New J. Phys. (1999), submitted for publication.
[9] H. Krömmer, A. Erbe, A. Tilke, S. Manus, R.H. Blick, Europhys. Lett. (1999), submitted for publication.
[10] H. Krömmer, Diploma Thesis, Ludwig-Maxmilians Universität München, 1999.
[11] B. Yurke, D.S. Greywall, A.N. Paragellis, P.A. Busch, Phys. Rev. A 51 (1995) 4211.
[12] A. Erbe, H. Krömmer, A. Kraus, R.H. Blick, G. Corso, K. Richter (1999), in preparation.
[13] R.A. Millikan, Phys. Rev. 32 (1911) 349.
[14] T.A. Fulton, G.J. Dolan, Phys. Rev. Lett. 59 (1987) 109.
[15] D.V. Averin, K.K. Likharev, J. Low Temp. Phys. 62 (1986) 345.
[16] P. Lafarge, H. Pothier, E.R. Williams, D. Esteve, C. Urbina, M.H. Devoret, Z. Phys. B 85 (1991) 327.
[17] M.W. Keller, J.M. Martinis, N.M. Zimmerman, A.H. Steinbach, Appl. Phys. Lett. 69 (1996) 1804.
[18] R.J. Schoelkopf, P. Wahlgren, A.A. Kozhevnikov, P. Delsing, D.E. Prober, Science 280 (1998) 1238.
[19] H. Birk, M.J.M. de Jong, C. Schönenberger, Phys. Rev. Lett. 75 (1995) 1610.
[20] L.Y. Gorelik, A. Isacsson, M.V. Voinova, B. Kasemo, R.I. Shekhter, M. Johnson, Phys. Rev. Lett. 80 (1998) 4526.
[21] Ch. Weiss, W. Zwerger, Europhys. Lett. 47 (1999) 97; cond-mat/9904149.